Journal of Materials Chemistry A

PAPER

View Article Online
View Journal | View Issue

Cite this: J. Mater. Chem. A, 2014, 2, 17031

Surface treated pollen performance as a renewable reinforcing filler for poly(vinyl acetate)†

Oluwatimilehin O. Fadiran and J. Carson Meredith*

Received 24th June 2014
Accepted 22nd August 2014

DOI: 10.1039/c4ta03219e

www.rsc.org/MaterialsA

Pollen grains have the potential to be effective plant-based biorenewable reinforcing fillers for polymers due to their high mechanical strength, chemical stability, and unique micro- and nano-structured surfaces. Pollen–polymer composites could form the basis for a new class of light-weight, high strength sustainable materials if compatible polymer–filler systems can be engineered. The exine shell of pollen, composed of sporopollenin, offers opportunities for surface functionalization to provide for compatibility between the pollen and the polymer matrix, but this idea has been previously unexplored. We present the first demonstration of surface functionalization of sporopollenin to enable incorporation of pollen as a reinforcing filler, using ragweed pollen in poly(vinyl acetate) (PVAc). Composites prepared with 'as received', untreated ragweed pollen displayed interfacial voids, degraded mechanical properties, and a decreased glass transition width with increased pollen loading, relative to neat PVAc. Composites prepared with pollen treated *via* an acid–base surface preparation displayed improved interfacial morphology and increasing modulus with pollen loading (29% increase). Interfacial adhesion was optimal for pollen functionalized with vinyltrimethoxysilane (VTMS), followed by *in situ* free radical polymerization of PVAc. *In situ* polymerization of functionalized pollen resulted in simultaneous stiffening and strengthening of composites (80% increase in tensile strength). Films containing treated and functionalized pollen also displayed a wider glass transition regions in the presence of pollen filler relative to neat PVAc.

Introduction

Particulate fillers are often incorporated into polymers in order to improve their mechanical, thermal, and optical properties, to name a few.[1–4] Many studies have demonstrated the successful use of non-biological materials ranging from inorganic particles, such as calcium carbonate, to carbon organic materials including carbon blacks and nanotubes as reinforcing fillers in fabricating polymer composites.[5–8] Many particulates are denser than the polymer, or are derived in a non-sustainable manner, and there is interest in finding lower density, sustainably sourced alternatives. In addition, most fillers are spherical or irregular spheroids, without significant capability to alter the particle fine surface features or geometry.

In contrast, pollen has the potential to be an effective biorenewable filler due to its high strength, chemical stability, low density and the unique architecture of its outer shell.[9–13] Besides being used directly as fillers, biological particulates such as pollen grains, bacteria, and viruses have attracted much research interest as templates for fabricating synthetic inorganic mimics that preserve their unique surface architectures.[9–11,14–16] These inorganic mimics may also function as fillers that combine biological architecture with synthetic chemistry. While some studies have investigated pollen grains, only one study has reported utilization of pollen as a filler.[17] Furthermore, pollens from sources such as ragweed plants are ubiquitous and inexpensive natural materials that are based on sustainable, non-food resources.

Pollen grains are the carrier of the male gametes for plant reproduction. A pollen grain is composed of an outer layer (exine) and an inner layer (intine).[18,19] The exine is composed of sporopollenin, a highly crosslinked organic substance consisting of fatty acids, phenylpropanoids, and phenolics.[20,21] Fig. 1 displays monomer and macromer components that have been confirmed in sporopollenin, such as long aliphatic chains, aromatic cross-linkers (mainly cinnamic acids), ether cross-linkages and ester functions.[22] The exine's chemical composition suggests compatibility with polymers capable of polar interactions. Underneath the exine layer, not exposed to the outer surface, lies the intine which is rich in cellulose and hemicelluloses. The cellular material carried within the grain is easily extracted using well known techniques, leaving behind a hollow, strong shell.

To date, the one known study that explored pollen grains as reinforcing fillers of polymers used solution casting of native,

School of Chemical and Biomolecular Engineering, Georgia Institute of Technology, 311 Ferst Drive NW, Atlanta, Georgia, 30332-0100, USA. E-mail: carson.meredith@chbe.gatech.edu

† Electronic supplementary information (ESI) available. See DOI: 10.1039/c4ta03219e

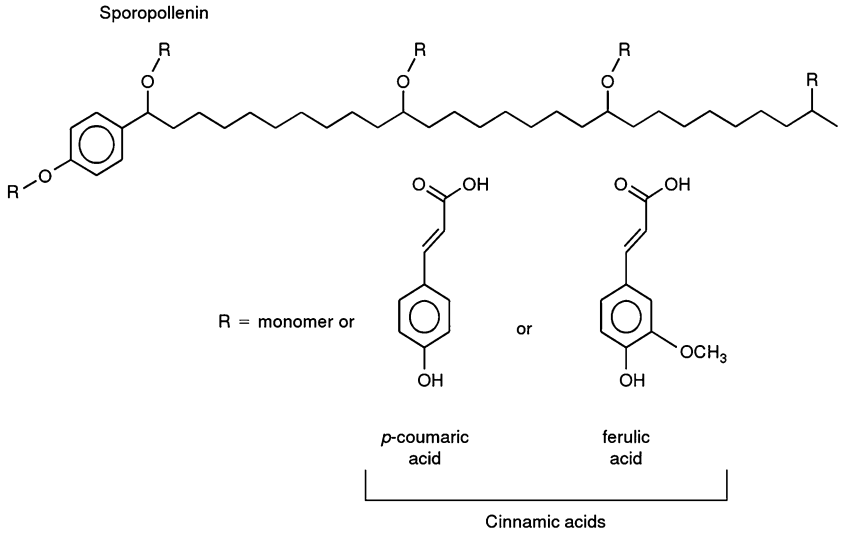

Fig. 1 Monomer and macromer precursors of sporopollenin.[22]

untreated ragweed pollen in polystyrene and polycaprolactone.[17] Interfacial voids between the polymer and pollen filler were reported to result in only small improvements in strain at break at low pollen loadings. One may expect that utilization of more polar polymers, as well as polymerizing monomer *in situ* in the presence of functionalized pollen may enhance interfacial compatibility. This can be rationalized by expected increased adhesion due to covalent binding of chains to the pollen surface as well as a decreased viscosity of the initial reaction mixture (relative to a solvent-casting solution).

To explore these ideas, in the present study pollen fillers were incorporated into a more polar matrix polymer than those previously explored, poly(vinyl acetate) (PVAc), by both solution casting and *in situ* free radical polymerization of vinyl acetate monomer (VAM). Short ragweed pollen (*A. artemisiifolia*) was selected as a model pollen grain because of its natural abundance, unique 'spiny' echinate surface morphology, and previously published adhesion data.[23,24] As received pollen was compared to pollen modified by two treatments: acid–base hydrolysis and functionalization with an organosilane. The effectiveness of pollen as a reinforcing and strengthening filler in PVAc was characterized by mechanical properties, interfacial morphology, and glass transition temperature of pollen–polymer composites as a function of pollen loading, processing method, and pollen treatment.

Experimental section

Materials

Defatted Short ragweed (D, *A. artemisiifolia*, Greer Laboratories) pollen grains were stored at 4 °C prior to use. VAM (Sigma Aldrich) was filtered through aluminum silicate to remove hydroquinone inhibitor. Azobisisobutyronitrile (AIBN, Sigma Aldrich) was of reagent grade and absolute ethanol was used as solvent. Potassium hydroxide (KOH, EMD Millipore) and phosphoric acid (H_3PO_4, BDH chemicals) were used for pollen treatment. Vinyltrimethoxysilane (VTMS, Sigma Aldrich) was used to functionalize the pollen surface. For solution processing, dichloromethane (DCM, Sigma Aldrich) was used as a solvent for PVAc (Sigma Aldrich, $M_w = 500\,000$).

Solution processing of pollen–PVAc composites

A measured mass of pollen was dispersed in DCM and sonicated for uniform dispersion. The desired mass of polymer was then added step wise to the solvent to make a 15 vol% PVAc solution. The mixtures were agitated on a rotational stirrer for 24 h. The solutions were cast on glass plates with a doctor blade, and slowly dried under a solvent saturated environment for 24 h. The films were dried under vacuum for 24 h at 90 °C. Samples were slowly cooled down to room temperature before peeling the films from the plates using a razor. Average film thicknesses were 130 μm ± 20 μm.

In situ polymerization of pollen–PVAc composites

AIBN (0.0135 g) was added to VAM (32.66 g) in a round bottom flask. After the AIBN dissolved, 15 mL of ethanol were also added to the flask. For composites, a measured mass of pollen grains (for composites containing 1–15 vol% of pollen) was dispersed in the ethanol and sonicated prior to addition to the flask, to ensure pollen dispersion. The flask was purged with nitrogen and the mixture was stirred at 75 °C for 2.5 h. The resulting solution mixtures were cast on glass plates with a doctor blade, and slowly dried under a solvent saturated environment for 24 h. The films were dried under vacuum for 24 h at 90 °C. Samples were slowly cooled down to room temperature before peeling the films from the plates using a razor.

Extraction of pollen cellular material

An acid–base treatment (hereafter labeled as AB) was used to clean and isolate the exine shell for incorporation in polymer films as well as to prepare them for further functionalization.[19,25]

Briefly, pollen was dispersed in 6 w/v% KOH solution for 24 hours while stirring. After washing the pollen with hot water, ethanol, and drying the pollen, it was dispersed in 85% H_3PO_4 for 7 days. This pollen was dried after washing with hot water, acetone, and ethanol. This process caused the pollen grains to lose ~80% of their original weight. AB pollen was incorporated in polymer films *via* the *in situ* polymerization mentioned above. Fig. 2 shows D pollen with intracellular material intact *versus* hollow AB pollen.

Silane functionalization of pollen grains

AB pollen was used as the starting point for functionalization with VTMS (hereafter referred to as ABV) to enable grafting of polymer chains to the pollen surface. AB pollen was heated under vacuum at 100 °C to remove adsorbed water then dispersed in toluene and sonicated. This solution was purged under nitrogen for 30 minutes while stirring. VTMS was added to the flask with a syringe through a rubber stopper. This solution was heated overnight and pollen was recovered after washing with toluene, hexane, and ethanol. ABV pollen was incorporated in polymer films *via* the *in situ* polymerization mentioned above. Fig. 3 shows a schematic for the reaction of VTMS with pollen hydroxyl groups and functionalized pollen's copolymerization with vinyl acetate monomer. Average film thicknesses were 160 μm ± 10 μm.

Sample types

The composite processing methods and pollen treatments explained above were combined into four different sample types that were characterized in this study. These samples were as follows: solution processed PVAc with native defatted pollen (S-D), polymerized PVAc with native defatted pollen (P-D), polymerized PVAc with acid–base pollen (P-AB), and polymerized PVAc with silane functionalized AB pollen (P-ABV).

Characterization

FTIR spectra were obtained on a Thermo Scientific spectrophotometer from 4000 cm^{-1} to 400 cm^{-1}. Pollen received as is, acid treated, and functionalized with VTMS were mixed with KBr powders and pressed in pellets for measurement. A high-throughput mechanical characterization (HTMECH) apparatus was used to measure mechanical properties including tensile strength, elastic modulus, and toughness, as described previously.[26] Briefly, the polymer films were mounted on a steel grid

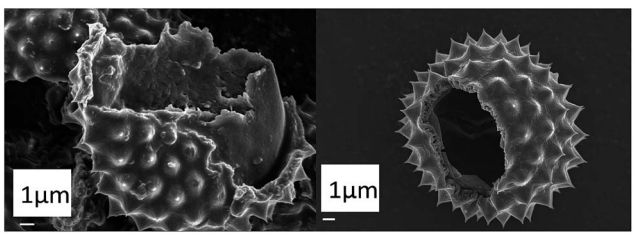

Fig. 2 Native D pollen (left) with intracellular material intact and hollow AB pollen (right).

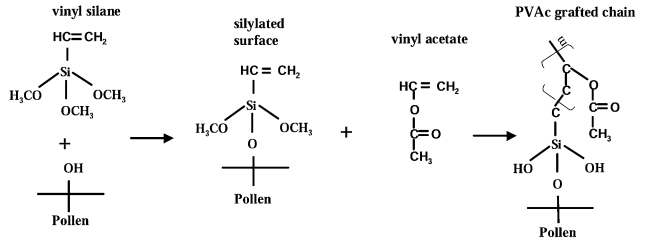

Fig. 3 Schematic of pollen surface functionalization and copolymerization of functionalized pollen with monomer (adapted from ref. 27).

and contacted with a steel pin with a 1.5 mm diameter hemispherical cap at a constant strain rate (0.5 mm s^{-1}). The pin is oriented normal to the film surface, resulting in equi-biaxial deformation. For each sample, an average thickness was obtained using 9 measurements with a micrometer, 9 stress–strain profiles were measured to failure, and mechanical properties of the films were obtained. All mechanical tests were performed under ambient conditions. Scanning electron microscopy (SEM) was performed with a Zeiss Ultra-60 FE-SEM instrument to examine the interfacial morphology of both freeze fractured and HTMECH fracture surfaces of the composites. Molecular weights of polymerized samples were measured by GPC. A Shimadzu liquid chromatograph was used with THF as the eluent. One Phenogel 5 μm linear column and one Phenogel 5 μm mixed bed column were calibrated with 10 PS standards samples from 500 to 1.2 × 10^6 g mol^{-1}. Differential scanning calorimetry (DSC) measurements were performed with a TA Instruments DSC Q200 in a nitrogen atmosphere, using specimens of 8–9 mg cut from films and sealed in aluminum pans with lids. Samples were heated from 10 to 80 °C, above T_g of the pure PVAc, at 20 °C min^{-1}, kept isothermal for 1 min, cooled down to 10 °C at 20 °C min^{-1}, and held isothermal for 1 min again. This cycle was repeated twice. T_g values were taken from the second cycle from the onset value of the tangents on the heat flow curves. The width of the glass transition region, ΔT_g, was taken as the difference between the endpoint and the onset temperatures. The density of materials was assessed by pycnometry in a 25 ml specific gravity bottle. Ethanol was used to determine the density of D and AB pollen and water was used to determine the density of neat PVAc and pollen–PVAc composites. A known mass of material, m_s, was added to the bottle of known mass (m_0). The liquid of known density was then added to bottle and the total mass, m_T, is measured. The density of the solid is given by:

$$\rho_s = m_s \Big/ \left(V - \frac{m_T - m_0 - m_s}{\rho_{H_2O}} \right) \quad (1)$$

where V is the volume of the flask.

Results and discussion

FTIR analysis

Fig. 4 shows the FTIR spectra of native pollen and pollen recovered following each chemical modification (D, AB, ABV,

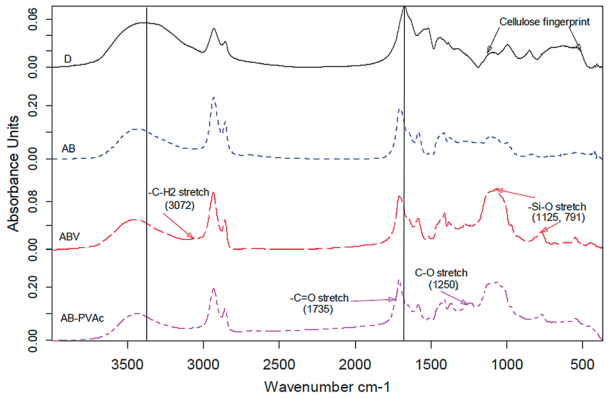

Fig. 4 FTIR spectra of pollen at various stages of surface treatment.

and AB-PVAc). The cellulose fingerprint in D pollen appears in the 1100 to 900 cm^{-1} region, due to the presence of polysaccharide material in the pollen intine.[21,28] The spectrum for AB pollen shows an important lack of peaks associated with polysaccharides in this range, indicating the full or partial dissolution the intine.[29,30] Additionally, D pollen displays a very broad band at 3375 cm^{-1} due to O–H stretching, having a stronger intensity than the –CH stretches of $–CH_2$ groups at 2910 and 2840 cm^{-1}. In contrast, AB pollen displays a more narrow –OH band with a smaller intensity than the $–CH_2$ peaks. AB pollen's OH band is also shifted to higher wavenumbers around 3450 cm^{-1}, indicating increased fractions of free hydroxyls. The C=O stretch of carboxyl groups also shifts from 1672 cm^{-1} to 1707 cm^{-1} in D and AB pollen, respectively. The acid–base hydrolysis decreases the ratio of hydroxyl to methylene groups, likely due to the dissolution of the strongly H-bonded cellulosic intine and results in higher fractions of free hydroxyl (not associated with the cellulose) and carboxyl groups in the sporopollenin, which would be more accessible for surface interactions with a composite matrix phase.

Silane functionalized pollen (ABV) spectra displayed a large band at 1125 cm^{-1} and a peak at 791 cm^{-1}, which are assigned to stretching vibration of Si–O–Si bonds.[31,32] There is an additional small peak at 3072 cm^{-1} assigned to the vinyl acetate groups on the silane.[33] These peaks indicate the successful attachment of silane to the pollen surface. Finally, pollen recovered from the copolymerization of ABV pollen with monomers displayed a peaks characteristic of PVAc at 1250 cm^{-1} and a shoulder peak at 1735 cm^{-1} assigned to stretching vibrations of C–O and C=O bonds, respectively.[34] These peaks confirm the successful functionalization of pollen with VTMS and the grafting of polymer chains to the pollen surface (AB-PVAc) following *in situ* vinyl acetate polymerization.

Interfacial morphology

Fig. 5–8 present the SEM images of freeze fractured and HTMECH fracture surfaces of pollen–PVAc composites. Fig. 5 shows the fracture surfaces for S-D films. Freeze fracture samples (5a and b) reveal the presence of interfacial voids between native D pollen and the polymer matrix. These voids

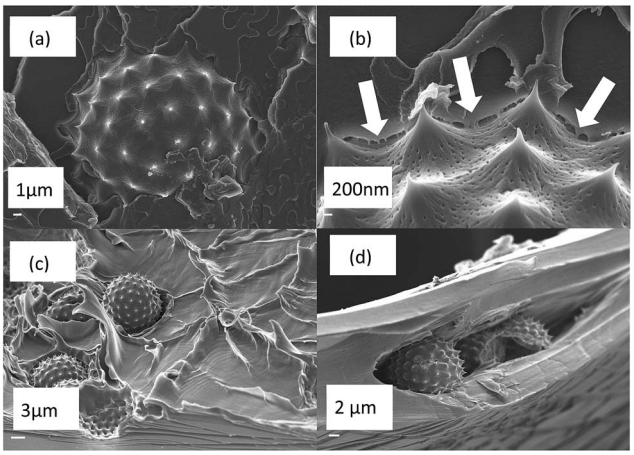

Fig. 5 S-D fracture surfaces. Freeze fractured cross sections (a and b) and HTMECH fracture surfaces (c and d). Arrows indicate polymer bridging.

appear smaller than the voids observed in our previous work utilizing less polar polystyrene and polycaprolactone, but are still present.[17] Thin polymer bridges at the pollen–polymer interface (5b) can be observed where the matrix has pulled away from the pollen surface. HTMECH fracture surfaces (5c and d) reveal that the pollen lies in void pockets of the polymer matrix and the pollen simply introduces voids in the material.

Fig. 6 shows similar results for P-D films. Freeze fracture samples still reveal voids surrounding some of the pollen grains (6a). However, some better adhered interfaces are present (6b). HTMECH fracture surfaces (6c and d) still show void pockets surrounding pollen grains and significant separation at the interface. The pockets are not as large as in the solution processed films (Fig. 5). However, polymerized films fractured at much lower stresses than solution processed films, so the smaller void pockets may be due to the smaller magnitudes of stress and deformation.

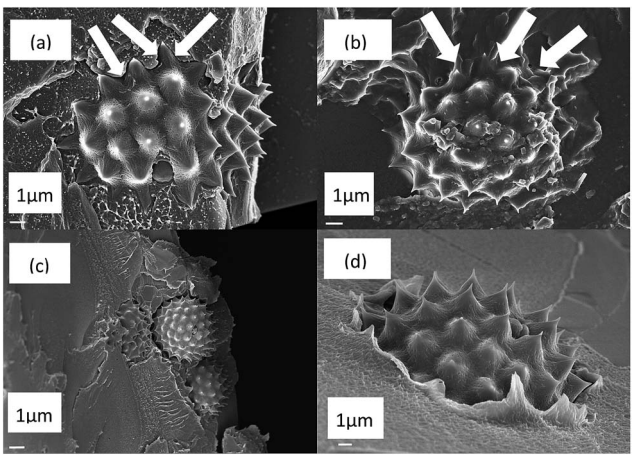

Fig. 6 P-D fracture surfaces. Freeze fractured cross sections (a and b). (a) Arrows indicate voids and (b) arrows indicate well adhered interfaces. HTMECH fracture surfaces (c and d).

Fig. 7 shows the fracture surfaces for P-AB films. Freeze fracture samples (7a and b) show an optimized interface for P-AB *versus* films S-D and P-D films, with a continuous interface between polymer matrix and pollen grains. No polymer bridging or interfacial voids are present surrounding pollen grains. HTMECH fracture surfaces (7c and d) further establish the optimized interface. Void pockets are no longer present with AB pollen that were present in films with D pollen. The optimized interface of P-AB films is likely due to increased specific interactions between the pollen surface and the polymer matrix. The acid–base treatment eliminates intracellular material (Fig. 2) that may block pollen surface hydroxyl and carboxyl groups. These exposed –OH and C=O functional groups likely increase hydrogen bonding (–OH) or dipole–dipole and van der Waals interactions with PVAc's carbonyls.[35,36] Additionally, additional hydroxyl groups may be generated on the pollen surface due to phosphorylation of hydroxyls and/or carboxyls,[30] thus increasing opportunities for adhesive interactions between pollen and the polymer matrix.

Fig. 8 shows the fracture surfaces for P-ABV films. Freeze fractured samples (8a and b) indicate that polymer coats the pollen surface and the pores of the pollen surface are less visible than previously observed due to this coating (8b). HTMECH fracture surfaces (8b and d) indicate the presence of deformed polymer that is still attached to the pollen after fracture. These images suggest that polymer is strongly attached to the pollen surface, possibly an indicator of successful grafting. Additional HTMECH fracture surfaces of all four samples can be found in supplementary material for further comparisons.

Mechanical properties

Fig. 9–12 show the mechanical properties obtained for the various pollen–PVAc composites. Fig. 9 shows properties for S-D films. Elastic modulus decreased continuously with increased pollen loading. Tensile strength and strain at break both increased slightly at low pollen loadings and then decreased continuously with increased pollen loading. The mechanical properties measured for S-D films are comparable to mechanical properties of PVAc and PVAc–zeolite composites previously measured with the HTMECH.[37] The properties of PVAc and PVAc–zeolite measured with HTMECH were also found to match properties measured with conventional tensile testing of the same films.

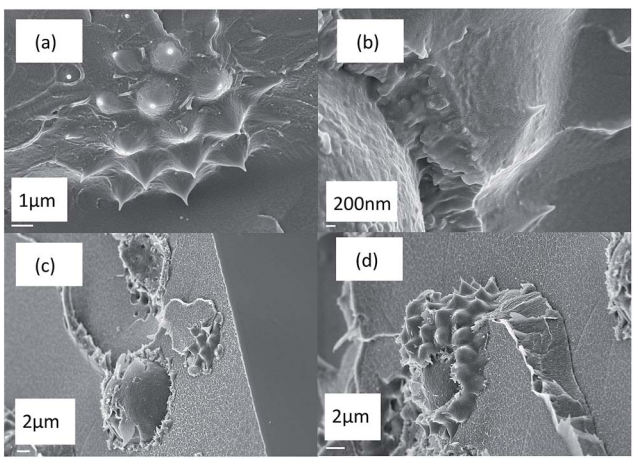

Fig. 7 P-AB fracture surfaces. Freeze fractured cross sections (a and b) and HTMECH fracture surfaces (c and d).

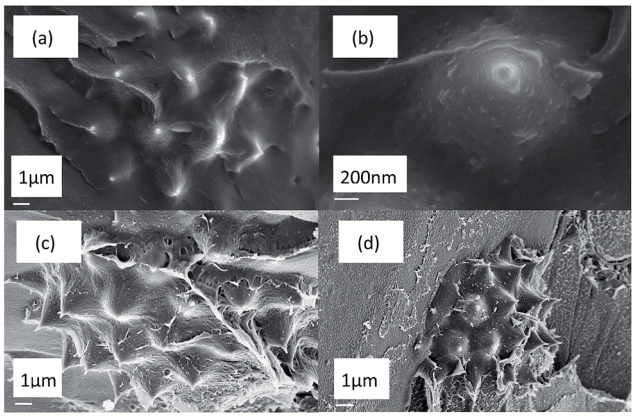

Fig. 8 P-ABV fracture surfaces. Freeze fractured cross sections (a and b) and HTMECH fracture surfaces (c and d).

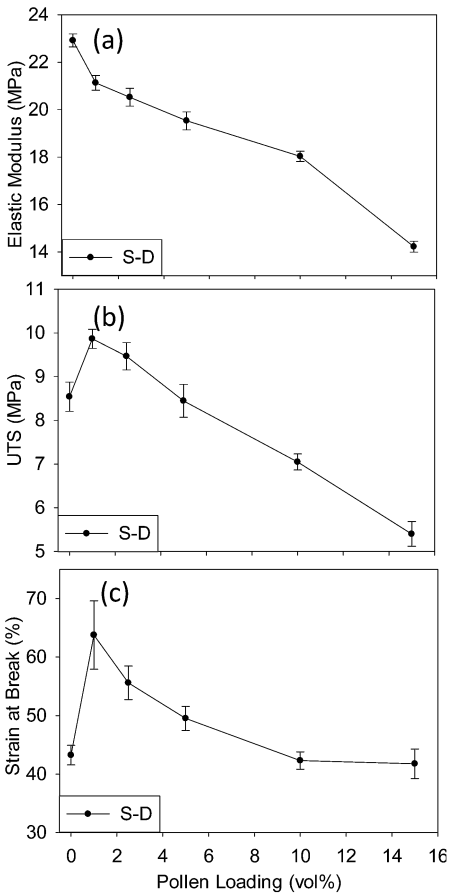

Fig. 9 Elastic modulus (a), UTS (b), and strain at break (c) of S-D composites. The error bars are 95% confidence intervals.

Fig. 10 shows similar trends in the properties for P-D films. The elastic modulus trend is slightly different than that of S-D films, with a possible small increase at low pollen loadings and a more gradual decline as pollen content increases further. Again, tensile strength and strain at break both increased slightly at low pollen loadings and then decreased continuously with increased pollen loading. The larger mechanical property values of S-D films *versus* polymerized films are due to the higher molecular weight of solution cast films (500 000 g mol^{-1}). The molecular weight of polymerized films was ~78 000 g mol^{-1} measured by gel permeation chromatography.

Properties for P-AB films are shown in Fig. 11. In contrast to S-D and P-D films, here, the elastic modulus increases with increasing loading. It is well-known that elastic modulus is independent of interfacial adhesion when it is measured at low deformations where interfacial separation does not occur.[3] As seen in Fig. 5 and 6, films with D pollen that display decreasing modulus also contain interfacial voids after preparation. Thus, an increasing loading of D pollen increases the amount of interfacial voids, decreasing the stiffness of the material.[38] On the other hand, films with AB pollen, which show increasing modulus, lack interfacial voids after preparation (Fig. 7). Thus, incorporation of AB pollen eliminates interfacial voids associated with untreated D pollen, which corresponds with increased material stiffness. Additionally, small increases in tensile strength and strain at break at low pollen loadings are absent. The continual decrease in these properties, as well as the lack of a toughening effect at low pollen loadings, further suggests the absence of interfacial voids. However, the decrease in tensile strength and strain at break with pollen loading indicate that the degree of adhesion between the phases is still low, although interfacial voids are not obvious in the SEM.

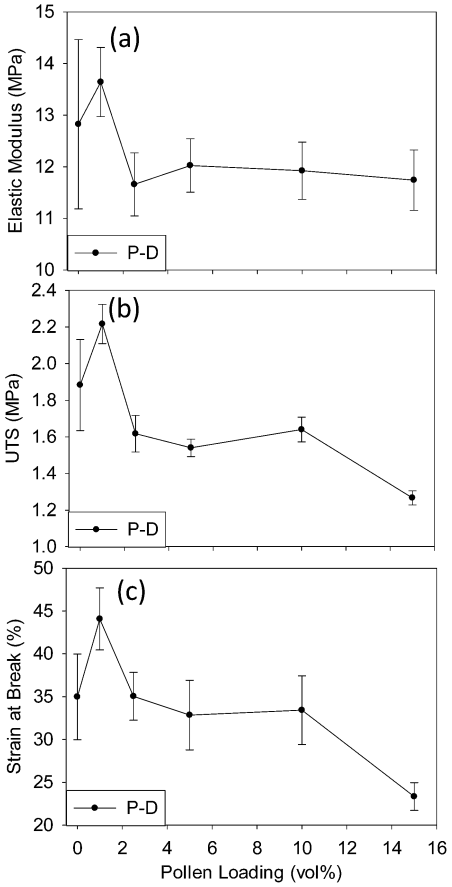

Fig. 10 Elastic modulus (a), UTS (b), and strain at break (c) of P-D composites. The error bars are 95% confidence intervals.

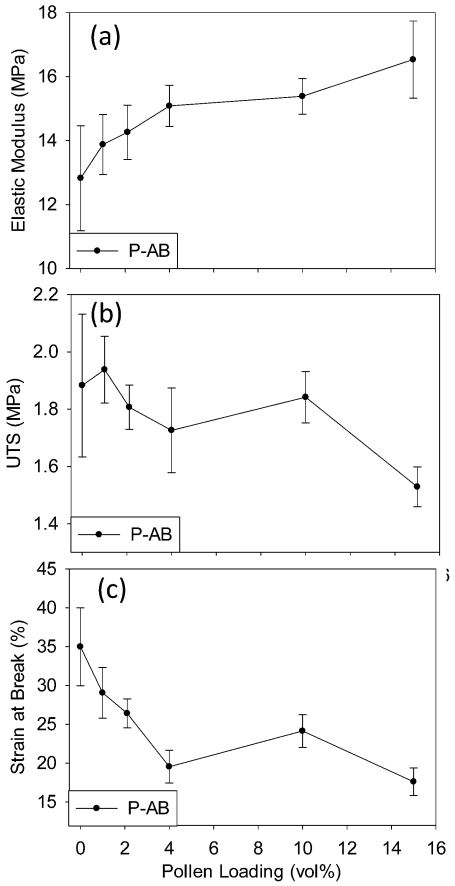

Fig. 11 Elastic modulus (a), UTS (b), and strain at break (c) of P-AB composites. The error bars are 95% confidence intervals.

Fig. 12 shows the properties of P-ABV films. Again, elastic modulus increases with increased pollen loading, similar to P-AB. In contrast with all other films, the tensile strength and strain at break of P-ABV films increase continually with increased pollen loading. This suggests that grafted polymer chains that are covalently bonded to the pollen surface are entangled with the chains of the polymer matrix. These mechanical observations and the proposed covalent-derived adhesion are consistent with the SEM evidence of strongly attached residual polymer at fracture surfaces (Fig. 8).

The stiffening effects observed in P-AB and P-ABV (Fig. 11a and 12a) films indicate that the pollen exine shell has a higher inherent modulus than the polymer matrix, although independent measurements of exine tensile modulus are not available. Both curves appear to approach a plateau at higher pollen loadings. A plateau is sometimes indicative of particle–particle interactions and agglomeration,[3] although this was not evident

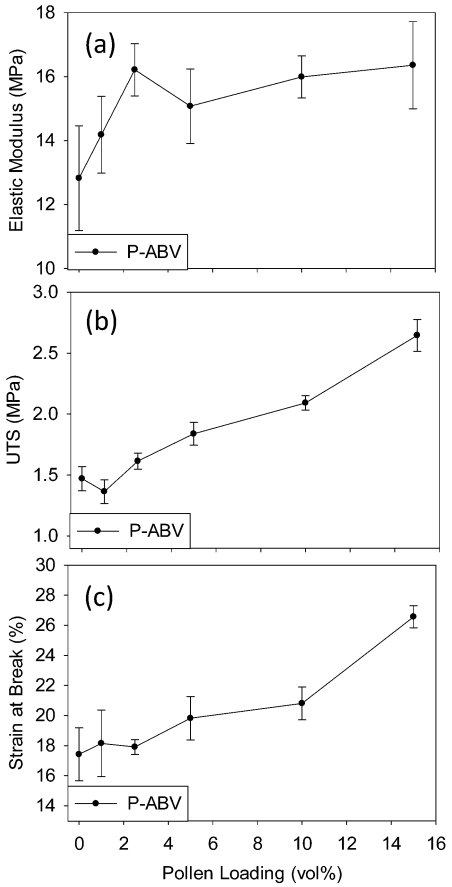

Fig. 12 Elastic modulus (a), UTS (b), and strain at break (c) of P-ABV. The error bars are 95% confidence intervals.

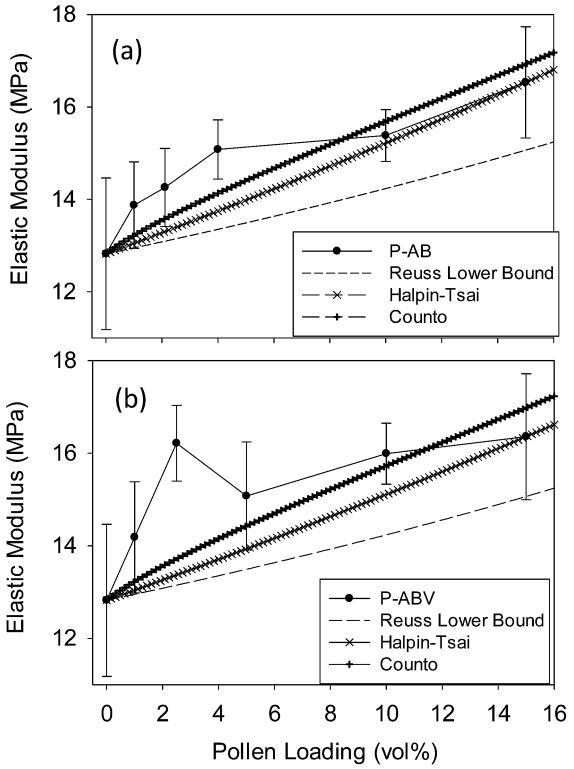

Fig. 13 Experimental data *versus* theories for elastic modulus: (a) P-AB and (b) P-ABV experimental modulus data.

from the SEM images. Although the pollen is micron sized, it introduces nanoscale spine features in the composite, which may allow particle–particle interactions at distances greater than expected based on the nominal particle diameter. There has been only one other study that reports a pollen modulus. This study reports the E_h (the product of a compressive elastic modulus and wall thickness) of desiccated ragweed pollen as 1653 N m^{-1} *via* micromanipulation techniques.[12] This results in a compressive modulus of 1653 MPa, using an approximate wall thickness of 1 micron for ragweed pollen. This value was used to compare the experimental modulus data to a lower bound model[3,39–41] for elastic modulus as shown in Fig. 13. The Reuss lower bound assuming iso-stress is given by the inverse rule of mixtures:

$$E_c^{lower} = E_f E_m / [E_f(1 - V_f) + E_m V_f] \quad (2)$$

where E_c^{lower}, E_f and E_m are the modulus of the composite, the filler, and the neat matrix respectively. V_f is the volume fraction of the filler. Fig. 13 shows that the experimental data for both P-AB and P-ABV films fall within the lower bound, when using the compressive pollen modulus of 1653 MPa. Although not shown here, the data also fell well into the Voigt upper bound, based on the rule of mixtures. Two models, Halpin–Tsai and Counto, which fall above the lower bounds, were fit to the experimental data in order to estimate the modulus of pollen.

The Halpin–Tsai semi-empirical model is shown in eqn (3).

$$E_c = E_m\left(\frac{1 + \eta\zeta V_f}{1 - \eta V_f}\right) \quad (3)$$

ζ and η are expressed as:

$$\zeta = 2 + 40V_f^{10} \quad (4)$$

$$\eta = \left(\frac{E_f}{E_m} - 1\right) \Big/ \left(\frac{E_f}{E_m} - \zeta\right) \quad (5)$$

The Halpin–Tsai model[3,40–42] predicted a modulus of 67.3 MPa for AB pollen and 62 MPa for ABV pollen *versus* the measured 12.8 MPa of the neat polymer. The largest percent errors were 8.8% and 17.5% for P-AB and P-ABV respectively. The Counto model,[3,43,44] shown in eqn (6), is a model for two phase particulate composites assuming a perfect bonding between filler and matrix and gives predictions in good agreement with a wide range of test data.

$$E_c = E_m\left[1 + V_f \Big/ \left(\sqrt{V_f} - V_f + \frac{E_m}{E_f - E_m}\right)\right] \quad (6)$$

As shown in Fig. 13, the Counto model, which is non-linear, provides a slightly better fit. The model predicted a modulus of 68.2 MPa for AB pollen and 69.8 MPa for ABV pollen *versus* the measured 12.8 MPa of the neat polymer. The largest percent errors were 6.3% and 15.4% for P-AB and P-ABV respectively. As expected, the predicted moduli of AB and ABV pollen are

comparable for both models because elastic modulus is independent of interfacial adhesion when it is measured at low deformations where interfacial separation does not occur.[3] The data is found to still fall above the lower bound when the estimates of pollen modulus from the Halpin–Tsai and Counto models are used as E_f. Additional models were considered such as the Takayanagi I,[45] which can account for decrease in reinforcement efficiency due to filler aggregation above percolation. However, in this case, pollen loadings are below percolation if they are considered as hard spheres ($V_f = 0.18$), so this model is not appropriate. Thus, the modelling shown here may overestimate the modulus of the pollen somewhat but is still useful due to the challenge of fitting data the displays plateauing behavior.

Thermal properties

Glass transition behavior was measured for the four different sample types as a function of pollen loading (0, 5, and 15 vol%). Little dependence was found of T_g values on pollen loading. However, the width of the glass transition region appears to correlate with the observed interfacial and mechanical properties. Table 1 reports the width of the glass transition region, ΔT_g, for the four different composites. Both S-D and P-D films display decreasing ΔT_g with increased pollen loading. The polymer chains at the polymer–pollen interface of these composites exhibit faster relaxation dynamics due to increased mobility of chains at the interfacial voids observed with SEM. Thus they display a decreasing trend in the width of the glass transition region. P-AB and P-ABV films display larger ΔT_g in the presence of pollen *versus* neat polymer. Here, the polymer chains at the polymer–pollen interface exhibit slower relaxation dynamics due to decreased mobility of chains at the interface.[46,47] This corresponds with the optimized interface (Fig. 7 and 8) and improved mechanical properties of these composites (Fig. 11 and 12). Polymer chains may show improved interactions with the AB pollen surface *versus* the D pollen surface due to increased specific interactions and/or improved van der Waals based compatibility, resulting in a larger width of the glass transition region in the presence of pollen filler. A similar result with ABV pollen is likely due to improved interactions of grafted polymer chains covalently bonded to the pollen surface that are able to entangle with the chains of the polymer matrix. Also, ΔT_g for P-AB and P-ABV films initially increase at lower loadings and then decrease at higher loadings, but still remain higher than the ΔT_g of the neat polymer. This may indicate an optimum loading exists where pollen filler has its maximum effect on ΔT_g. At higher loadings, particle–particle interactions become more likely which could decrease pollens overall effect on ΔT_g because of a reduction in pollen–PVAc interface. This may also play a role in the plateauing behavior observed for P-AB and P-ABV modulus. At higher loadings, the contribution of the pollen–PVAc interface to increased modulus may be lessened compared to the contribution at lower loadings where particle–particle interactions do not reduce the pollen–PVAc interfacial area.

Density of materials

Using pycnometry, the density of D was measured as 1.305 g cm^{-3}, while the density of AB pollen was measured as 1.165 g cm^{-3}. The intracellular material present in D pollen makes it denser than the hollow AB pollen as seen in Fig. 2. The native D pollen is much less dense than widely used fillers in industry, such as talc ($\rho = 2.75$ g cm^{-3}) and calcium carbonate ($\rho = 2.71$ g cm^{-3}), and has a density comparable to advanced fillers such as carbon nanotubes (ρ = 1.3–1.4 g cm^{-3}), cellulose (ρ = 1.5 g cm^{-3}) and starch (ρ = 1.5 g cm^{-3}). Interestingly, the hollow shells of AB pollen have a density that is lower than all of these fillers. Fig. 14 shows AB and D pollen dispersed in a PVAc–ethanol solution. D pollen settles out of solution in a matter of days. However, AB pollen remains well dispersed in solution for several months, further indicating the decreased density of AB pollen *versus* D Pollen.

Pycnometry was also used to determine the densities of the neat PVAc and pollen–PVAc composites. Neat PVAc's density was measured as 1.195 g cm^{-3}, matching its reported value of 1.19 g cm^{-3}. P-D and P-AB film densities were measured as 1.269 g cm^{-3} and 1.183 g cm^{-3}, respectively. AB pollen decreased the material density by 1.04% at 15 vol% pollen loading *versus* neat PVAc. Thus, unlike many other fillers would, pollen did not significantly impact the low density of the PVAc

Fig. 14 AB pollen dispersed in PVAc solution after several months (left) and D pollen settled out of PVAc.

Table 1 Width of glass transition regions (ΔT_g) of pollen–PVAc composites

Pollen loading (vol%)	S-D ΔT_g (°C)	P-D ΔT_g (°C)	P-AB ΔT_g (°C)	P-ABV ΔT_g (°C)
0	8.81	6.44	6.44	6.44
5	6.44	6.33	8.12	7.83
15	4.57	5.06	7.03	7.37

matrix. Also, interesting future work may involve sealing AB pollen and trapping air within the shells, which would allow for larger density reductions.

Conclusions

In this study, the effect of ragweed pollen loading on the mechanical, interfacial, and thermal properties of PVAc composites prepared by a solution processing and free radical polymerization casting method was investigated. Native pollen (D) was observed to introduce interfacial voids in both solution processed and polymerized composites. These interfacial voids resulted in degraded mechanical properties at high pollen loadings and a decreasing width of the glass transition region. Treatment of pollen *via* an acid–base hydrolysis method (AB) improved the interfacial adhesion relative to D pollen, likely the result of improved interactions between AB pollen and the PVAc matrix. Eliminating interfacial voids resulted in stiffening of the composite due to the addition of pollen filler, indicating that pollen has a relatively higher elastic modulus than the PVAc matrix. However, the degree of adhesion between AB pollen and PVAc matrix was still too low to allow for strengthening, indicated by decreasing material strength with increased pollen loading. Interfacial adhesion was further improved by functionalizing AB pollen with a vinyl silane in order to graft polymer chains on the pollen surface. Tensile strength and strain at break of films prepared with P-ABV increased with increased pollen loading, indicating a higher degree of adhesion than P-AB. Composites with both AB and ABV pollen displayed a wider glass transition region in the presence of pollen filler, compared to D pollen. These results indicate that pollen is a promising plant-based filler for reinforcing polymers, but that surface functionalization is a likely necessity to achieve significant improvements. Because functionalization appears to be an effective strategy, it would also be interesting to investigate other polymers that are reactive with hydroxyl groups, *e.g.*, urethanes and epoxies. In addition, the unique variety of nano- and micro-structures on pollens (as a function of plant species) creates an opportunity to use pollen as a model particulate to elucidate the effect of complex filler geometries on the wetting and adhesion of fillers.

Acknowledgements

We would like to thank the Renewable Bioproducts Institute (Georgia Institute of Technology) and the Air Force Office of Scientific Research (Grant # FA9550-10-1-0555) for financial support of this research.

Notes and references

1 R. T. Limited, *High Performance Fillers 2005: Cologne*, Germany, 8-9 March 2005, Rapra, 2005.
2 G. Wypych, *Handbook of Fillers, 3e*, ChemTec Publishing, 2010.
3 S.-Y. Fu, X.-Q. Feng, B. Lauke and Y.-W. Mai, *Composites, Part B*, 2008, **39**, 933–961.
4 B. J. Ash, D. F. Rogers, C. J. Wiegand, L. S. Schadler, R. W. Siegel, B. C. Benicewicz and T. Apple, *Polym. Compos.*, 2002, **23**, 1014–1025.
5 S. Lučić, V. Kovačević and D. Hace, *Int. J. Adhes. Adhes.*, 1998, **18**, 115–123.
6 Z. Spitalsky, D. Tasis, K. Papagelis and C. Galiotis, *Prog. Polym. Sci.*, 2010, **35**, 357–401.
7 P. H. T. Vollenberg and D. Heikens, *J. Mater. Sci.*, 1990, **25**, 3089–3095.
8 W. Wang, P. Ciselli, E. Kuznetsov, T. Peijs and A. H. Barber, *Philos. Trans. R. Soc., A*, 2008, **366**, 1613–1626.
9 S. R. Hall, H. Bolger and S. Mann, *Chem. Commun.*, 2003, 2784–2785.
10 S. R. Hall, V. M. Swinerd, F. N. Newby, A. M. Collins and S. Mann, *Chem. Mater.*, 2006, **18**, 598–600.
11 M. Jenik, A. Seifner, P. Lieberzeit and F. Dickert, *Anal. Bioanal. Chem.*, 2009, **394**, 523–528.
12 T. Liu and Z. Zhang, *Biotechnol. Bioeng.*, 2004, **85**, 770–775.
13 B. J. R. Thio, J.-H. Lee and J. C. Meredith, *Environ. Sci. Technol*, 2009, **43**, 4308–4313.
14 C. Feng and L. Dong-Xu, *Biomed. Mater.*, 2009, **4**, 025009.
15 Y. Wang, Z. Liu, B. Han, Y. Huang and G. Yang, *Langmuir*, 2005, **21**, 10846–10849.
16 Y. Wang, Z. Liu, B. Han, Z. Sun, J. Du, J. Zhang, T. Jiang, W. Wu and Z. Miao, *Chem. Commun.*, 2005, 2948–2950.
17 J. H. Lee, B. M. Suttle, H. J. Kim and J. C. Meredith, *Macromol. Mater. Eng.*, 2011, **296**, 1055–1062.
18 P. Piffanelli, J. H. E. Ross and D. J. Murphy, *Sex. Plant Reprod.*, 1998, **11**, 65–80.
19 R. Wiermann and S. Gubatz, *International Review of Cytology-a Survey of Cell Biology*, 1992, **140**, 35–72.
20 S. Blackmore, A. H. Wortley, J. J. Skvarla and J. R. Rowley, *New Phytol.*, 2007, **174**, 483–498.
21 E. Dominguez, J. A. Mercado, M. A. Quesada and A. Heredia, *Sex. Plant Reprod.*, 1999, **12**, 171–178.
22 A. R. Hemsley and I. Poole, *The Evolution of Plant Physiology*, Elsevier Science, 2004.
23 B. J. R. Thio, J. H. Lee and J. C. Meredith, *Environ. Sci. Technol.*, 2009, **43**, 4308–4313.
24 H. Lin, I. Gomez and J. C. Meredith, *Langmuir*, 2013, **29**, 3012–3023.
25 D. Southworth, *Am. J. Bot.*, 1974, **61**, 36–44.
26 J.-L. Sormana, S. Chattopadhyay and J. C. Meredith, *Rev. Sci. Instrum.*, 2005, **76**, 062214–062219.
27 Y. Cohen, 1997, p. Medium: ED; Size: 12 pages.
28 E. Domínguez, J. A. Mercado, M. A. Quesada and A. Heredia, *Grana*, 1998, **37**, 93–96.
29 G. Shaw and D. C. Apperley, *Grana*, 1996, **35**, 125–127.
30 S. Barrier, in *Chemistry*, The University of Hull, 2008.
31 S. L. Blagojević, V. Kovačević, M. Leskovac, D. Vrsaljko, V. Volovšek and C. Nover, *e-Polym.*, 2013, **13**, 384–397.
32 J. He, Y. Shen, D. G. Evans and X. Duan, *Composites, Part A*, 2006, **37**, 379–384.
33 R. Di Maggio, S. Dirè, E. Callone, F. Girardi and G. Kickelbick, *Polymer*, 2010, **51**, 832–841.

34 M. Leskovac, V. Kovačević, S. Lučić Blagojević, D. Vrsaljko and V. Volovšek, *e-Polymers*, 2004, 348.
35 F. M. Fowkes, *J. Adhes. Sci. Technol.*, 1987, **1**, 7–27.
36 F. M. Fowkes, D. O. Tischler, J. A. Wolfe, L. A. Lannigan, C. M. Ademu-John and M. J. Halliwell, *J. Polym. Sci., Polym. Chem. Ed.*, 1984, **22**, 547–566.
37 J.-H. Lee, P. Zapata, S. Choi and J. C. Meredith, *Polymer*, 2010, **51**, 5744–5755.
38 L. Liu, B.-M. Zhang, D.-F. Wang and Z.-J. Wu, *Compos. Struct.*, 2006, **73**, 303–309.
39 J. S. Bergström and M. C. Boyce, *Rubber Chem. Technol.*, 1999, **72**, 633–656.
40 U. Delawa, *Delaware Composites Design Encyc: Micromechanical Materials Model*, Taylor & Francis, 1990.
41 M. A. Islam and K. Begum, *Prediction Models for the Elastic Modulus of Fiber-reinforced Polymer Composites: An Analysis*, 2011.
42 Y.-P. Wu, Q.-X. Jia, D.-S. Yu and L.-Q. Zhang, *Polym. Test.*, 2004, **23**, 903–909.
43 R. F. M. Bakker, *J. Am. Concr. Inst.*, 1983, **80**, 345–345.
44 I. E. A. Yoshitake, F. Rajabipour, Y. Mimura and A. Scanlon, *Advances in Civil Engineering*, 2012, **2012**, DOI: 10.1155/2012/391214.
45 M. R. Loos and I. Manas-Zloczower, *Macromol. Theory Simul.*, 2012, **21**, 130–137.
46 D. Fragiadakis, L. Bokobza and P. Pissis, *Polymer*, 2011, **52**, 3175–3182.
47 C. G. Robertson and C. M. Roland, *Rubber Chem. Technol.*, 2008, **81**, 506–522.